Study of Bifurcations in Current-Programmed DC/DC Boost Converters: From Quasi-Periodicity to Period-Doubling

William C. Y. Chan and Chi K. Tse, *Senior Member, IEEE*

***Abstract*— This paper studies the bifurcation paths exhibited by a simple second-order dc/dc boost converter under current-programmed control with and without voltage feedback. Previous work in this area has reported two distinct types of bifurcation paths, namely via *regions* of *quasi-periodic orbits* and *period-doubling.* This paper demonstrates that the two different types of bifurcation paths can, in fact, be viewed as part of another bifurcation in which the quasi-periodic sequence transmutes into the period-doubling sequence, and that such a bifurcation is observed regardless of the presence of the outer voltage feedback loop as long as a suitable set of bifurcation parameters is chosen. The describing iterative map is derived in closed form and is used to develop the main results via a series of computer experiments. The characteristic multipliers are calculated and the first onset of flip-bifurcation is predicted. Computer simulation based on an exact piecewise switched model confirms the predicted bifurcations. The exhibition of quasi-periodic orbits is confirmed by computation of the Lyapunov exponent. Finally, a series of return maps are generated to provide an alternative viewpoint to the reported bifurcations in terms of a transmutation from a tent-like map to a logistic-like map.**

***Index Terms*— Bifurcation chaos, boost converter, current-programmed control.**

I. Introduction

CURRENT-PROGRAMMED control, being one of the most commonly used control schemes in dc/dc converters, has received much attention from power electronics engineers in the past two decades [1]–[5]. As is the rule rather than the exception for any new control application, much of the study reported so far has focused on the design of the involving feedback loops and performance evaluation on the basis of small-signal models, presumably because such kinds of practical-oriented study tend to yield immediate rewards and are usually quite tractable. Detailed nonlinear dynamics and potential modes of instability of current-programmed dc/dc converters, though being important issues with subtle and long-term practical implications, do not seem to attract as much attention as they deserve. Recently, chaos from dc/dc converter circuits under current-programmed control has been studied [6]–[10]. Two distinct types of bifurcation paths have been identified for such circuits, namely, one that goes through *a region of quasi-periodicity* [6]–[8]), and one that goes through *period-doubling* [9], [10]. The work of [6] is based on a fourth-order Ćuk converter, whereas those of [8], [9], and [10] are based on a second-order boost converter.

Our objective in this paper is to put together the previously observed bifurcation paths, and view them as part of another bifurcation arising from variation of a suitably chosen parameter. In other words, we will study the bifurcations at two abstract levels. At each level, a different bifurcation parameter is used. We refer to the bifurcation parameter used in the previous studies as the *primary bifurcation parameter*, based on which we observe either quasi-periodicity or period-doubling. We will define another bifurcation parameter, which we refer to as *secondary bifurcation parameter*, and based on which we observe a "super"-bifurcation that leads quasi-periodicity to period-doubling.

We will present our results as follows. In Section II, the operation of the boost converter under current programmed control is explained and the *exact* state equation describing the system is derived. As a prelude to the main discussion, some computer-generated waveforms will be shown in Section III to illustrate the various possible operating regimes of current-programmed dc/dc converters. In Section IV, an iterative map is derived in closed form which will be used in Section V to develop the main results regarding the bifurcations of the open-loop system. The characteristic multipliers are computed in Section V-B, from which the onset of the first flip bifurcation is predicted. Using the same iterative map, a series of bifurcation diagrams are generated in Section V-C, corresponding to different values of the secondary bifurcation parameter. "Exact" computer simulations presented in Section V-D yield similar bifurcation diagrams. The same exercise is repeated in Section VI for a practical version of the system, in which an additional voltage feedback loop is included for load regulation. Here, with a different set of primary and secondary bifurcation parameters, we again observe similar routes to chaos via regions of quasi-periodicity and period-doubling, as well as the same bifurcation from quasi-periodicity to period-doubling as in the case of the open-loop system. In order to confirm the exhibition of quasi-periodic orbits, the Lyapunov exponents are computed in Section VII. For a certain range of the primary bifurcation parameter lying between periodicity and chaos, the Lyapunov exponent takes the value of zero. Finally, in Section VIII, we generate a series of return maps

Manuscript received January 8, 1996; revised December 1, 1996. This work was supported by the Hong Kong Research Grants Council under a competitive-bid earmarked research grant. This paper was recommended by Associate Editor T. Endo.

The authors are with the Department of Electronic Engineering, Hong Kong Polytechnic University, Hung Hom, Hong Kong.

Publisher Item Identifier S 1057-7122(97)08045-8.

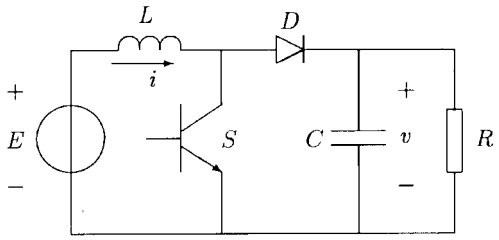

Fig. 1. The boost converter.

numerically to show the transition from a tent-like map to a logistic-like map. This provides a convenient viewpoint to the reported phenomena.

II. Operation of the Current-Programmed Boost Converter

The boost converter is a second-order circuit comprising an inductor, a capacitor, a diode, and with the load resistance connected in parallel with the capacitor. Fig. 1 shows the basic circuit. When operating in continuous mode, two switch states can be identified: 1) Switch S on and diode D off and 2) Switch S off and diode D on. The two switch states toggle periodically. We assume that the circuit takes switch state one for $nT \le t < (n+d)T$, and switch state two for $(n+d)T \le t < (n+1)T$, where n is an integer, d is the duty cycle, and T is the period.

A. Exact State Equations

The boost converter circuit described above can be regarded as a *variable structure* that toggles its topology according to the states of the switches. The boost converter operating in continuous mode can thus be described by the following sequence of state equations:

$$\begin{aligned} \dot{x} &= A_1 x + B_1 E, \qquad \text{for } nT \le t < (n+d)T \\ \dot{x} &= A_2 x + B_2 E, \qquad \text{for } (n+d)T \le t < (n+1)T \end{aligned} \quad (1)$$

where x denotes the state vector of the circuit, i.e., $x = [v\, i]^T$ and, in particular, the A's and B's in (1) are given by

$$A_1 = \begin{bmatrix} -1/RC & 0 \\ 0 & 0 \end{bmatrix} \quad B_1 = \begin{bmatrix} 0 \\ 1/L \end{bmatrix} \quad (2)$$

when the switch is in state one, and

$$A_2 = \begin{bmatrix} -1/RC & 1/C \\ -1/L & 0 \end{bmatrix} \quad B_2 = \begin{bmatrix} 0 \\ 1/L \end{bmatrix} \quad (3)$$

when the switch is in state two. The solution to (1) can be obtained analytically or via a numerical algorithm such as the Runge–Kutta algorithm. Simulation of the cycle-by-cycle time-domain waveforms is possible using the above piecewise switched model. We will base all our simulations on this model.

B. Review of Current-Programmed Control

The subject of investigation is a current-programmed switching converter. The schematic diagram is shown in Fig. 2. The inductance current is chosen as the programming

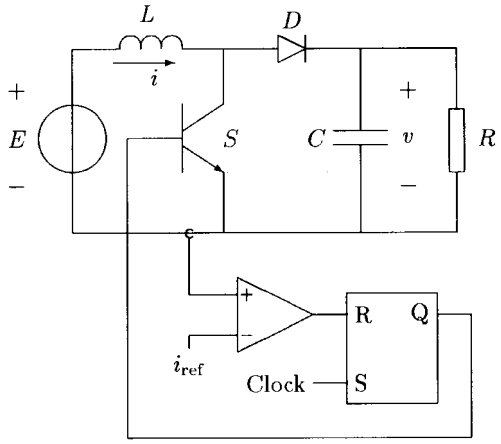

Fig. 2. Schematic of current-programmed boost converter.

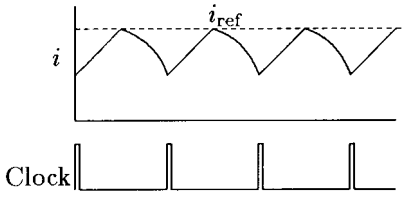

Fig. 3. Waveform of inductance current.

variable, which by comparing with a reference current i_{ref} generates the on–off driving signal for switch S. Specifically, switch S is turned on at the beginning of the cycle, i.e., at $t = nT$. The inductance current increases while switch S is on. As i climbs to the value of i_{ref}, switch S is turned off, and remains off until the next cycle begins. A typical waveform of the inductance current is shown in Fig. 3. It should be noted that although an inner current loop always exists, the circuit is regarded as an open-loop system when the value of i_{ref} is fixed, i.e., in the absence of an outer voltage feedback loop. However, in practice, an outer voltage feedback loop is usually included for the purpose of load regulation, which forces the value of i_{ref} to be a function of the output voltage v. In this case, the converter is said to be under a closed-loop current-programmed control. In this paper, we will study both the cases with and without the voltage feedback loop, and show that the bifurcation from quasi-periodicity to period-doubling occurs regardless of the presence of the outer voltage loop. Furthermore, in the authors' other publications [11]–[13], the same bifurcation from quasi-periodicity to period-doubling is also observed for the buck converter.

III. A Glimpse at the Nonlinear Behavior of Current-Programmed Converters

Before embarking on a detailed study of the various routes to chaos in current-programmed converters, let us take a quick tour of some typical operating regimes of a boost converter under current-programmed control. The sample waveforms shown in the following subsections are derived from the *exact* piecewise switched model described in Section II-A. Note that we have included a duty cycle limiter in our simulations such

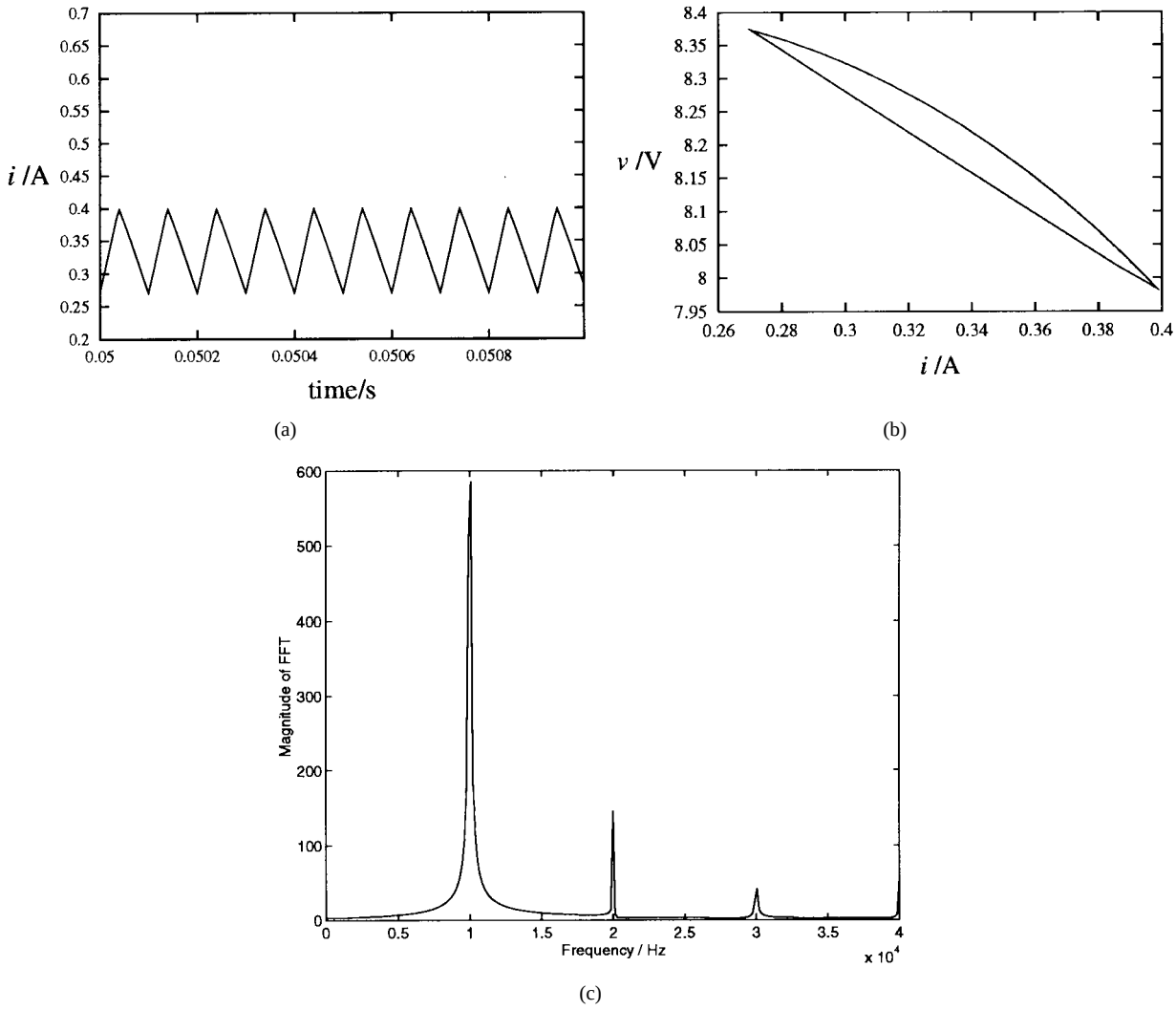

Fig. 4. Fundamental periodic operation. (a) Time-domain waveform, (b) phase portrait, and (c) FFT spectrum of the waveform in (a).

that $d \leq 0.9$. This will prevent the switch from being closed for the entire period (i.e., continuously being closed for more than one period) in the case where the reference current is large, as will be manifested in the following simulated waveforms. Such an arrangement is also commonly found in practical implementation.

A. Fundamental and Subharmonic Orbits

The most common and perhaps the only acceptable operating regime employed in practical power supplies is the fundamental periodic regime. Fig. 4(a) shows the inductance current waveform of a typical current-programmed converter under a fundamental periodic operation. The corresponding phase portrait and the FFT spectrum are shown in Fig. 4(b) and (c), which demonstrate the stable and periodic nature of the system. Note that a fundamental operation is possible when $i_{\rm ref}$ is sufficiently small. Moreover, when $i_{\rm ref}$ is not small, many other operating regimes are possible. For example, Figs. 5 and 6 show period-two and period-four subharmonic operation, respectively. It is worth noting that subharmonic operations have never been considered in the practical design of power supplies despite the fact that they are stable.

B. Quasi-Periodic Orbits

Fig. 7(a) shows a quasi-periodic waveform. (This particular example is a quasi-$4T$ periodic waveform.) The corresponding phase portrait is shown in Fig. 7(b). In a later section, we will compute the value of the Lyapunov exponent under this operating regime and confirm the exhibition of quasi-periodicity. Due to its nonperiodic nature, this type of operation tends to induce noises, some of which fall in the audible range, and is thus rather undesirable for practical use [see Fig. 7(c)]. Partly for this reason, this type of operation has never been allowed in the final product, although it is frequently encountered by engineers during the development stage of a power supply.

C. Chaotic Orbits

The current waveform, phase portrait, and corresponding FFT spectrum of the waveform for the circuit operating chaotically are shown in Fig. 8. The spectrum has a continuous and broad-band nature. Needless to say, conventional power-supply designers have always banned this type of operation in their final products, although they could hardly avoid encountering it in their workbench.

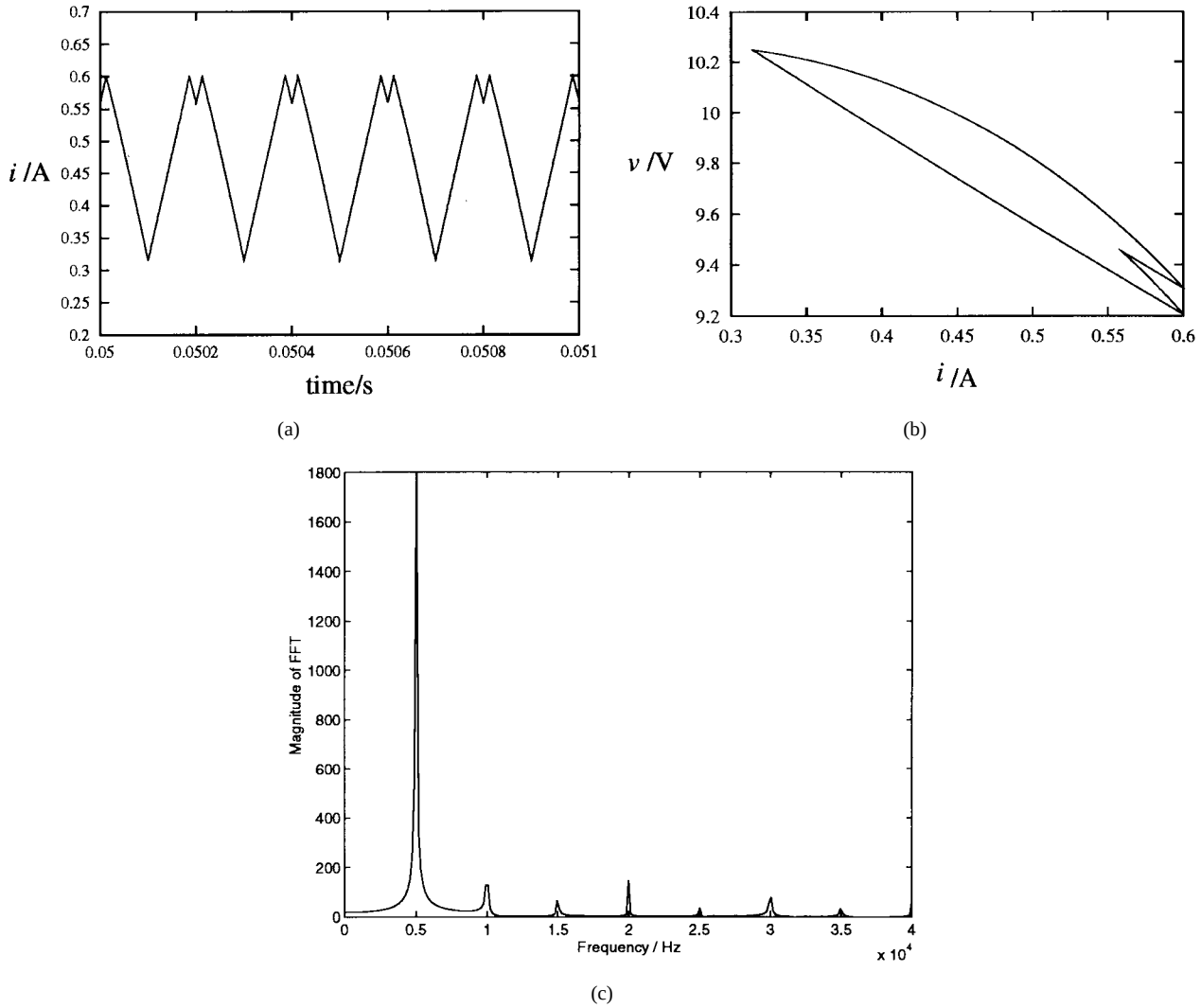

Fig. 5. $2T$ subharmonic operation. (a) Time-domain waveform, (b) phase portrait, and (c) FFT spectrum of the waveform in (a).

In the sequel we will systematically study these operating regimes and, in particular, we will investigate how the choice of parameters and their values can determine the type of operation of a current-programmed boost converter.

IV. Derivation of the Iterative Map For Current-Programmed Boost Converter

Our purpose in this section is to derive a difference equation for the system which takes the form

$$x_{n+1} = f(x_n, i_{\text{ref}}) \tag{4}$$

where $x = [v\, i]^T$ and subscript n denotes the value at the beginning of the nth cycle, i.e., $x_n = x(nT)$.

As mentioned in Section II-A, the state equation for the circuit in any switch state can be written in the form $\dot{x} = A_j x + B_j E$, where A_j and B_j are the system matrices in switch state j, and E is the input voltage. Using a successive substitution method, the value of x_{n+1} can be expressed in terms of x_n and the duty cycle d_n:

$$\begin{aligned} x_{n+1} &= \Phi_2(T - d_nT)\Phi_1(d_nT) \\ &\quad \cdot \left[x_n + \int_{nT}^{nT+d_nT} \Phi_1(nT - \tau) B_1 E . d\tau \right] \\ &\quad + \Phi_2(T - d_nT) \int_{nT+d_nT}^{(n+1)T} \Phi_2(nT + d_nT - \tau) B_2 E . d\tau \end{aligned} \tag{5}$$

where $\Phi_j(\xi)$ is the transition matrix corresponding to A_j and is given by

$$\Phi_j(\xi) = \mathbf{1} + \sum_{k=1}^{\infty} \frac{1}{k!} A_j^k \xi^k, \qquad \text{for } j = 1, 2. \tag{6}$$

If a truncated series is used for Φ_j, an approximate iterative map may be obtained which takes the form

$$\begin{bmatrix} v_{n+1} \\ i_{n+1} \end{bmatrix} = \begin{bmatrix} f_{11}(d_n) & f_{12}(d_n) \\ f_{21}(d_n) & f_{22}(d_n) \end{bmatrix} \begin{bmatrix} v_n \\ i_n \end{bmatrix} + \begin{bmatrix} g_1(d_n) \\ g_2(d_n) \end{bmatrix} E. \tag{7}$$

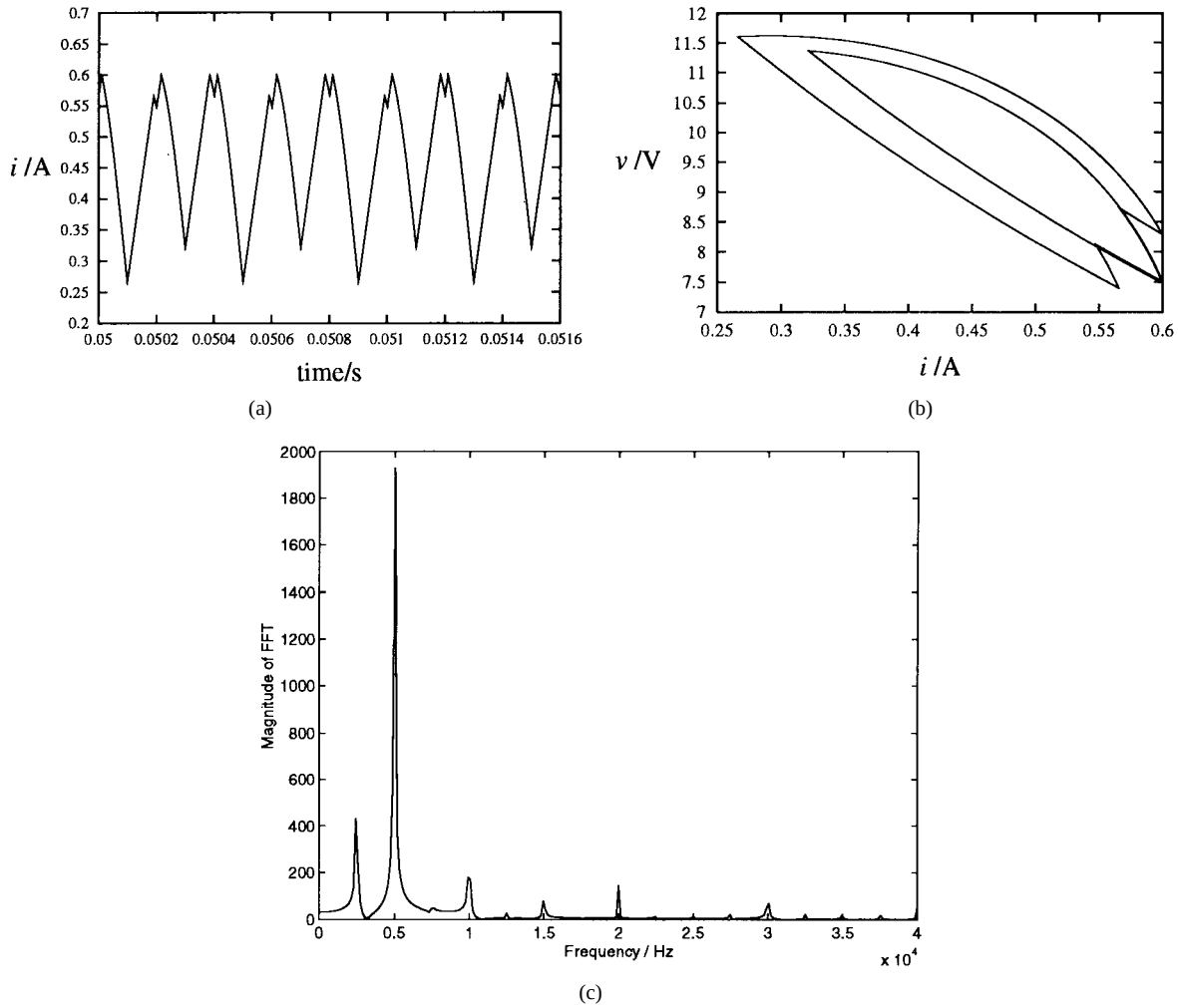

Fig. 6. $4T$ subharmonic operation. (a) Time-domain waveform, (b) phase portrait, and (c) FFT spectrum of the waveform in (a).

The expressions of the $f(.)$'s and the $g(.)$'s are given in the Appendix.

Since a difference equation of the form (4) is desired, d_n should be expressed in terms of $i_{\rm ref}$. By inspection of the circuit and the inductor current waveform, we have

$$L\frac{dt}{dt} = L\frac{i_{\rm ref} - i_n}{d_n T} = E \tag{8}$$

$$\Longrightarrow \quad d_n = \frac{i_{\rm ref} - i_n}{(E/L)T}, \tag{9}$$

Clearly (7) and (9) combine to give the required iterative map. We will use them to predict the chaotic behavior of the system. Wherever possible, we will attempt to calculate the characteristic multipliers in order to locate possible onsets of flip bifurcation. To get better ideas of the possible routes to chaos and their relationship with the parameter values, we resort to numerically calculating the sequence of x_n. Stable periodic or chaotic orbits may emerge after a sufficiently large number of iterations. Moreover, the order of periodicity can be easily checked by inspecting the sequence. In the next section we will study the various routes to chaos and their controlling parameters for the open-loop system. The study of the closed-loop system will be postponed to Section VI.

V. The Open-Loop System

A. Overview of the Routes to Chaos and Choice of Bifurcation Parameters

In [7]–[10], $i_{\rm ref}$ has been chosen as a bifurcation parameter. Essentially, by varying $i_{\rm ref}$ we would observe the way the circuit changes its qualitative behavior from a fundamental stable system to a chaotic system. We refer to $i_{\rm ref}$ as the *primary bifurcation parameter*. As reported previously in [6]–[10], routes to chaos via quasi-periodic orbits and period-doubling are possible. However, there has been no attempt to find out the condition that determines the type of the route to chaos for a given set of parameters. In fact, our main result in this paper addresses this important issue. To this end we introduce a *secondary bifurcation parameter* γ, which is defined as

$$\gamma = \frac{T}{CR}. \tag{10}$$

We will show later that as γ increases, the route to chaos initially goes through quasi-$4T$-periodic orbits, then goes through quasi-$8T$-periodic orbits, and continues to go through

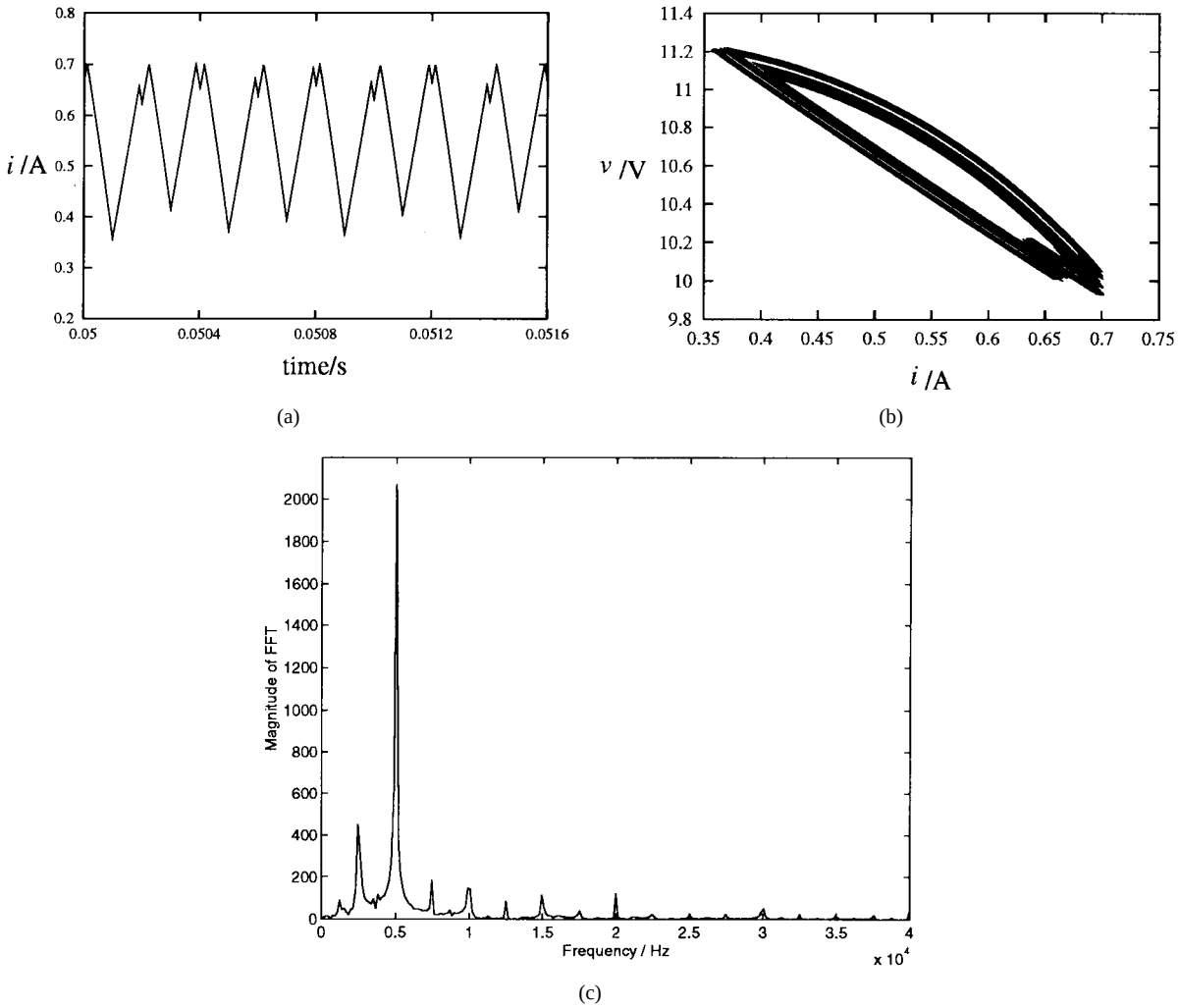

Fig. 7. Quasi-4T subharmonic operation. (a) Time-domain waveform, (b) phase portrait, and (c) FFT spectrum of the waveform in (a).

quasi-periodic orbits of 16T, etc. It eventually becomes period-doubling for large values of γ. Fig. 9 depicts a panoramic view of the main result to be reported in this paper. As shown in this figure, for small values of the secondary parameter, the route to chaos (with respect to the primary parameter) is via quasi-4T-periodic orbits. As we increase the secondary parameter, the quasi-4T-periodic orbits become stable 4T subharmonic orbits, and the route to chaos is via quasi-8T-periodic orbits. Eventually, for large values of the secondary parameter, the system exhibits a well-known period-doubling route to chaos.

B. Calculation of Characteristic Multipliers

In this section, we examine the characteristic multipliers of the system, from which we can rigorously locate the onset of the first flip bifurcation (i.e., from period-one to period-two orbits). Essentially, we consider the iterative function $f(.)$ of (4), and compute its characteristic multipliers corresponding to any given fixed point X_Q. The first flip bifurcation occurs when one of the characteristic multipliers equals -1. Likewise, computation of the characteristic multipliers of the function $f[f(.)]$ can locate the onset of the second flip bifurcation (i.e., from period-two to period-four orbits) if it exists.

The characteristic multipliers of an iterative function $f(.)$ are the roots λ of the characteristic equation

$$\det\left[\lambda \mathbf{1} - J_F(X_Q)\right] = 0. \tag{11}$$

where $J_F(X_Q)$ is the Jacobian of $f(.)$ evaluated at the fixed point X_Q. In the case of our boost converter under current-programmed control, the function $f(.)$ can be written in the following form:

$$x_{n+1} = f(x_n, i_{\text{ref}}) = \begin{bmatrix} f_1(v_n, i_n, i_{\text{ref}}) \\ f_2(v_n, i_n, i_{\text{ref}}) \end{bmatrix}. \tag{12}$$

From (7), we have

$$f_1(.) = f_{11}(d_n)v_n + f_{12}(d_n)i_n + g_1(d_n)E \tag{13}$$

$$f_2(.) = f_{21}(d_n)v_n + f_{22}(d_n)i_n + g_2(d_n)E \tag{14}$$

where d_n is, in turn, a function of i_{ref}, as given in (9). Hence, the Jacobian $J_F(X_Q)$ is given by

$$J_F(X_Q) = \begin{bmatrix} \dfrac{\partial f_1(.)}{\partial v_n} & \dfrac{\partial f_1(.)}{\partial i_n} \\ \dfrac{\partial f_2(.)}{\partial v_n} & \dfrac{\partial f_2(.)}{\partial i_n} \end{bmatrix}_{x_n = X_Q} \tag{15}$$

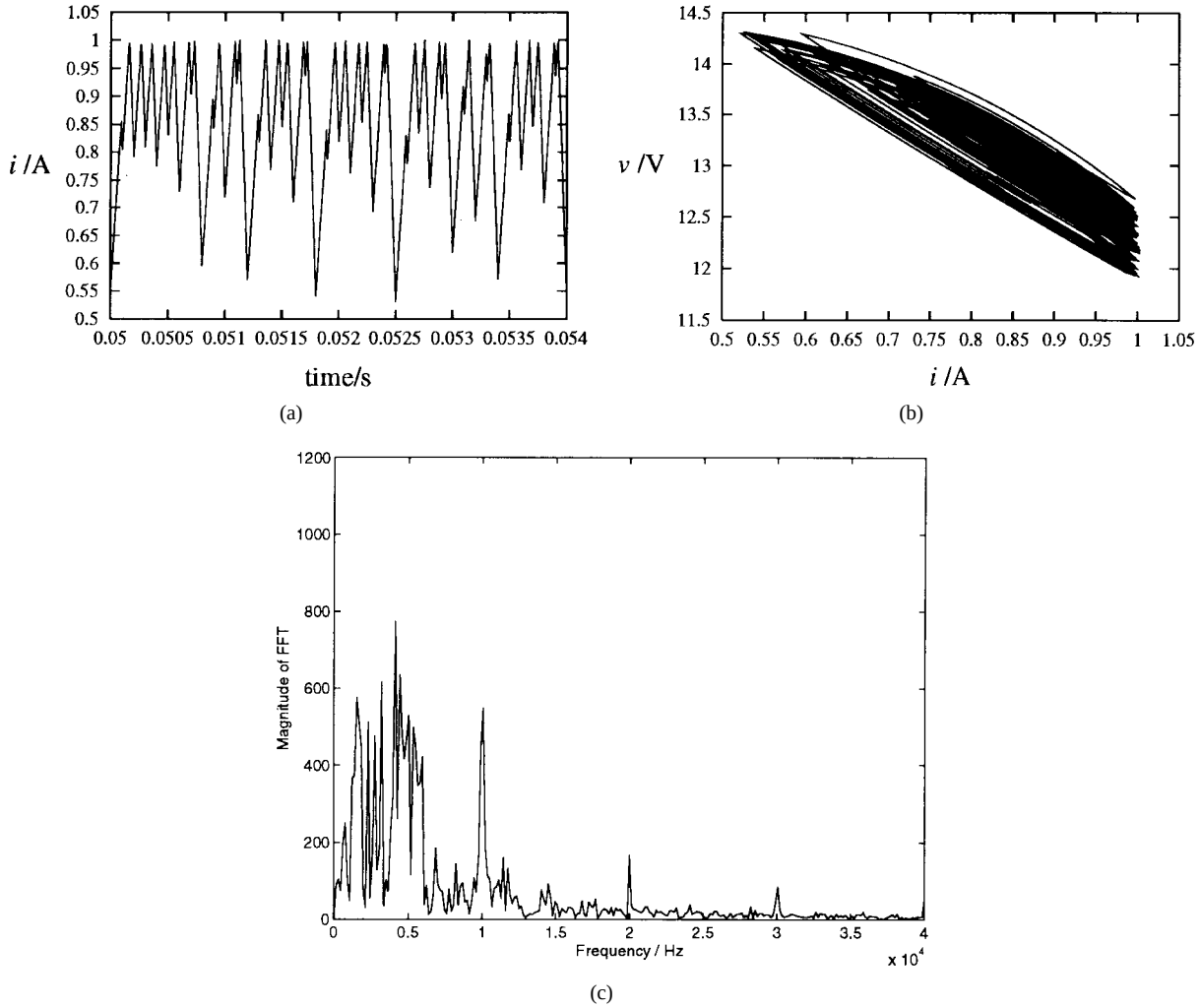

Fig. 8. Chaotic operation. (a) Time-domain waveform, (b) phase portrait, and (c) FFT spectrum of the waveform in (a).

where

$$\frac{\partial f_1(.)}{\partial v_n} = f_{11}(d_n) + v_n f'_{11}(d_n)\frac{dd_n}{dv_n} + i_n f'_{21}(d_n)\frac{dd_n}{dv_n} + Eg'_1(d_n)\frac{dd_n}{dv_n} \tag{16}$$

$$\frac{\partial f_1(.)}{\partial i_n} = v_n f'_{11}(d_n)\frac{dd_n}{di_n} + f_{12}(d_n) + i_n f'_{12}(d_n)\frac{dd_n}{di_n} + Eg'_1(d_n)\frac{dd_n}{di_n} \tag{17}$$

$$\frac{\partial f_2(.)}{\partial v_n} = f_{21}(d_n) + v_n f'_{21}(d_n)\frac{dd_n}{dv_n} + i_n f'_{22}(d_n)\frac{dd_n}{dv_n} + Eg'_2(d_n)\frac{dd_n}{dv_n} \tag{18}$$

$$\frac{\partial f_2(.)}{\partial i_n} = v_n f'_{21}(d_n)\frac{dd_n}{di_n} + f_{22}(d_n) + i_n f'_{22}(d_n)\frac{dd_n}{di_n} + Eg'_2(d_n)\frac{dd_n}{di_n}. \tag{19}$$

The characteristic multipliers can now be computed by first finding the fixed point corresponding to any given i_{ref} using the Newton–Raphson method or otherwise [14], and then solving the characteristic equation (11).

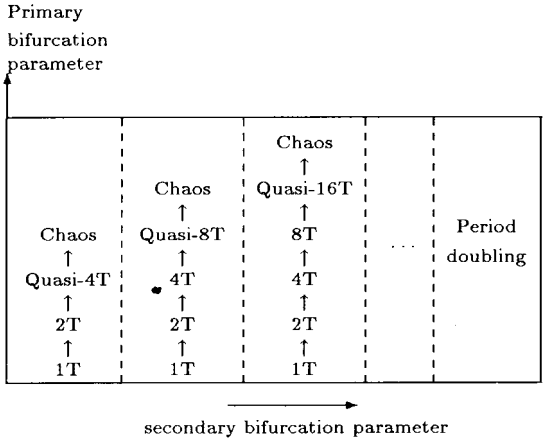

Fig. 9. Outline of primary and secondary bifurcations.

We now attempt to use the characteristic multipliers to predict the occurrence of flip bifurcation. The general procedure will be exemplified here using the set of circuit parameters listed in Table I, with the capacitor value chosen for $\gamma = 0.125$. To keep our discussion concise, we will omit details of calculations of the characteristic multipliers, but focus mainly on the cases in the vicinity of the first flip

bifurcation. Specifically we report our calculations in Table II, and summarize the trend of the locus as follows (see also Fig. 10).

1) For small $i_{\rm ref}$ (less than 0.497), the magnitudes of the characteristic multipliers are less than one, implying stable period-one orbits.
2) As $i_{\rm ref}$ increases, one of the characteristic multipliers goes toward -1, and at $i_{\rm ref} \approx 0.497$, the characteristic multipliers are -1 and 0.752 484, implying a flip bifurcation at this value of $i_{\rm ref}$.
3) For $i_{\rm ref} > 0.497$, the iterative function $f(.)$ is unstable. We consider instead the function $f[f(.)]$, denoted by $f^2(.)$. In a likewise fashion, we can compute the fixed point (actually two alternate fixed points) of $f^2(.)$, and the characteristic multipliers. In this particular case, right after the first flip, the characteristic multipliers jump to about 1 and 0.575, and gradually move toward each other.
4) When $i_{\rm ref} \approx 0.516$, the two real characteristic multipliers collide and break off to become a complex conjugate pair.
5) Calculations are no longer possible for a slight increase of $i_{\rm ref}$ beyond 0.596. Our algorithms involve determination of the steady-state fixed points from the time series. However, when $i_{\rm ref} > 0.596$, the series becomes a periodic having no fixed points. Evaluation of the required Jacobian thus becomes impossible. (Note: Difficulties in the computation of characteristic multipliers for other power electronics systems have also been reported by other authors [10], [15].)
6) At the point where the $2T$ orbit loses stability, the norm of the complex characteristic multipliers is approximately 0.74, which is far from the boundary of the unit circle. Thus, we are not able to see the movement of the characteristic multipliers across the boundary of the unit circle, as would be expected from a typical Neimark–Sacker bifurcation [16]. (Note: Such a jump from stable operation to instability or possible chaos will also be shown in Section VII in the light of Lyapunov exponents.)

The above results give a partial picture of the bifurcation path exhibited by the system for a particular value of the secondary bifurcation parameter. In the following subsection we attempt to provide (by a series of computer experiments) a fuller picture regarding the possible routes to chaos exhibited by the system under study.

C. Bifurcation Diagrams Derived from the Iterative Map

Based on (7) and (9), we can obtain the discrete time values of x at $t = nT$ for all n. In particular, if we allow the iteration to proceed for a sufficiently long time, the sequence may either diverge, converge to a periodic orbit, or be attracted to a chaotic orbit. In our numerical experiments, the values of the components are chosen to ensure that the circuit operates theoretically in the continuous mode, as listed in Table I. Our experiments with this iterative map have led to the bifurcation diagrams shown in Fig. 11. The transition

TABLE I
CIRCUIT PARAMETERS

Circuit Components	Values
Switching Period T	100μs
Inductance L	1.5mH
Load Resistance R	40Ω
Input Voltage E	5V

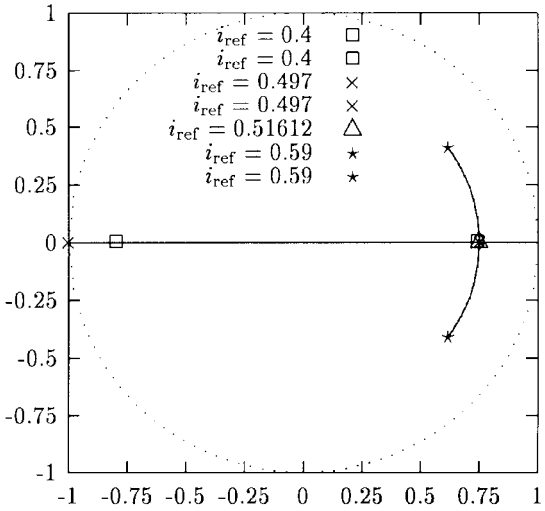

Fig. 10. Locus of characteristic multipliers for $\gamma = 0.125$.

TABLE II
CHARACTERISTIC MULTIPLIERS FOR $\gamma = 0.125$

$i_{\rm ref}$	Char. mult.	Norm	Remarks
0.4	$-0.796317, 0.743175$	–	Stable 1T
0.45	$-0.901889, 0.748953$	–	Stable 1T
0.497	$-1, 0.752484$	–	Flip
0.5	$0.985136, 0.575415$	–	Stable 2T
0.51	$0.887391, 0.636454$	–	Stable 2T
0.512	$0.861104, 0.655413$	–	Stable 2T
0.514	$0.828361, 0.680837$	–	Stable 2T
0.51612	$0.755725, 0.745718$	–	Stable 2T
0.52	$0.743632 \pm j0.0990274$	0.750197	Stable 2T
0.53	$0.7254 \pm j0.186191$	0.748914	Stable 2T
0.54	$0.707215 \pm j0.242556$	0.747654	Stable 2T
0.55	$0.689074 \pm j0.286867$	0.746402	Stable 2T
0.56	$0.670968 \pm j0.324089$	0.745139	Stable 2T
0.57	$0.652892 \pm j0.356432$	0.743849	Stable 2T
0.58	$0.634837 \pm j0.385116$	0.742518	Stable 2T
0.59	$0.6168 \pm j0.410884$	0.741126	Stable 2T

of the bifurcation path from one that goes through quasi-$4T$-periodic orbits via progressively longer quasi-periodic orbits to one that goes through period-doubling is summarized as follows.

Observation 1: $\gamma = 0.125$

As shown in Fig. 11(a), the circuit goes through stable $1T$ orbits, stable $2T$ orbits, quasi-$4T$ orbits, and eventually exhibits chaos.

Observation 2: $\gamma = 0.25$

The bifurcation path with respect to $i_{\rm ref}$, after the stable $1T$ and $2T$ regions, enters a region of stable $4T$ orbits (instead of quasi-$4T$), and then quasi-$8T$, and eventually chaos. The bifurcation diagram is shown in Fig. 11(b), a blow-up of which is shown in Fig. 12(a).

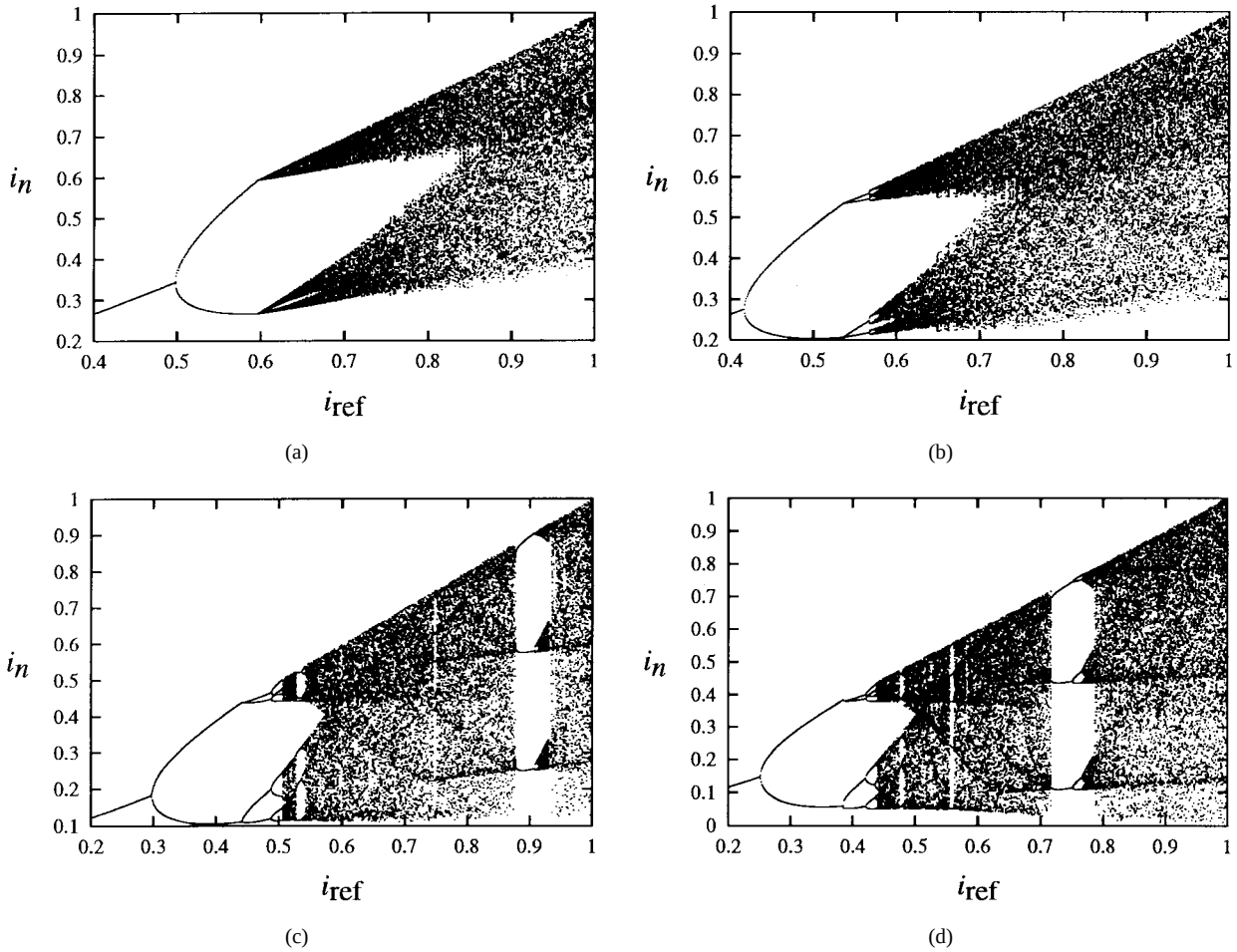

Fig. 11. Bifurcation diagrams using the iterative map. (a) Via quasi-4T orbits ($\gamma = 0.125$). (b) Via quasi-8T orbits ($\gamma = 0.25$). (c) Via quasi-16T orbits ($\gamma = 0.48$). (d) Via period-doubling ($\gamma = 0.625$).

Observation 3: $\gamma = 0.48$

The bifurcation diagram is shown in Fig. 11(c). An enlargement is shown in Fig. 12(b). Here the bifurcation path goes through a region of quasi-16T orbits before it enters the chaotic region.

Observation 4: $\gamma = 0.625$

For this value of γ, the circuit follows a typical period-doubling route to chaos, as shown in Fig. 11(d).

Remarks: Up to this point, we have not provided any proof to the quasi-periodicity claimed above for certain regions of the bifurcation diagrams. Indeed, judging from the bifurcation diagrams such as the ones shown in Fig. 11, quasi-periodicity is not at all conclusive. Specifically, based only on the appearance of Fig. 11(a), there is no sufficient evidence to claim that quasi-4T orbits exist in the parameter range around $0.6 < i_{\text{ref}} < 0.66$. The only conclusive claim is that values visited by the sequence of points i_n are confined to four open regions. The orbit can be chaotic if the four regions are visited irregularly. Moreover, quasi-periodicity can exist if the sequence of i_n visits the four regions in a regular pattern, one after another in a fixed order. Thus, in order to be conclusive about the exhibition of quasi-4T orbits in the range of $0.6 < i_{\text{ref}} < 0.66$ in Fig. 11(a), we need to inspect the time-domain waveform and find out if it is "nearly 4T." For this particular case, we can refer to Fig. 7(a) for verification.

To verify quasi-periodicity, in Section V-C we will compute the Lyapunov exponent for the entire range of the bifurcation and demonstrate that the condition for quasi-periodicity, i.e., a zero largest Lyapunov exponent, is indeed satisfied.

D. Verification by "Exact" Computer Simulations

In this section, we verify the results reported in Section V-C by computer simulations. As mentioned in Section II, simulation based on the model of Section II-A gives the true waveforms of the circuit. The simulated waveforms can be used to generate bifurcation diagrams. Specifically, a large number of the current waveforms are simulated for a range of values of i_{ref}. The values of the current at $t = nT$ are extracted from each waveform, with the initial transient discarded. A bifurcation diagram can be obtained by plotting the discrete current values against i_{ref}. The bifurcation diagrams shown in Fig. 13 agree with the predicted bifurcation diagrams developed earlier by the iterative map, except that the predicted patterns are slightly shifted to the right. Such discrepancy is due to the use of a truncated Taylor series in the derivation of the iterative map.

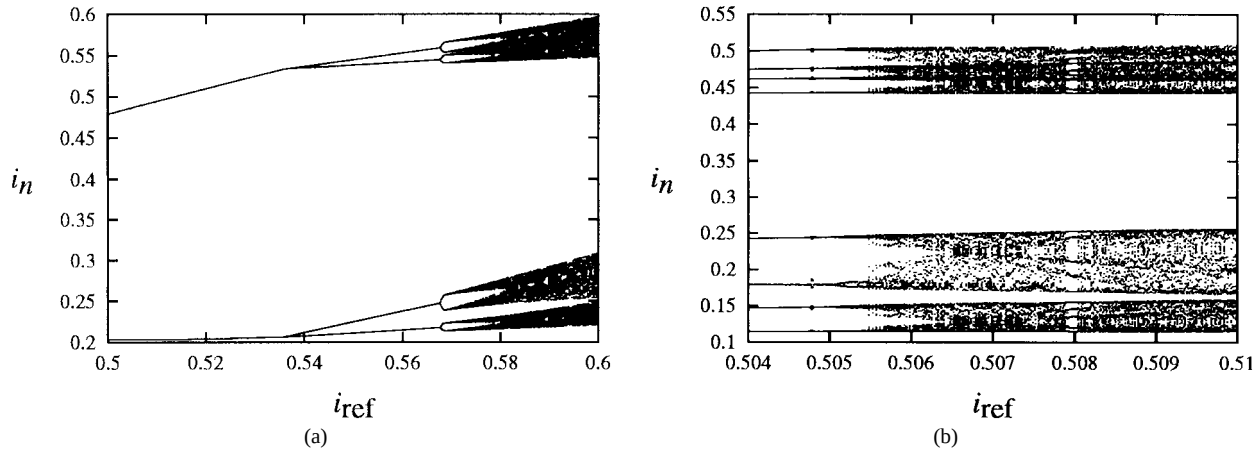

Fig. 12. (a) Zoom-in of Fig. 11(b). (b) Zoom-in of Fig. 11(c).

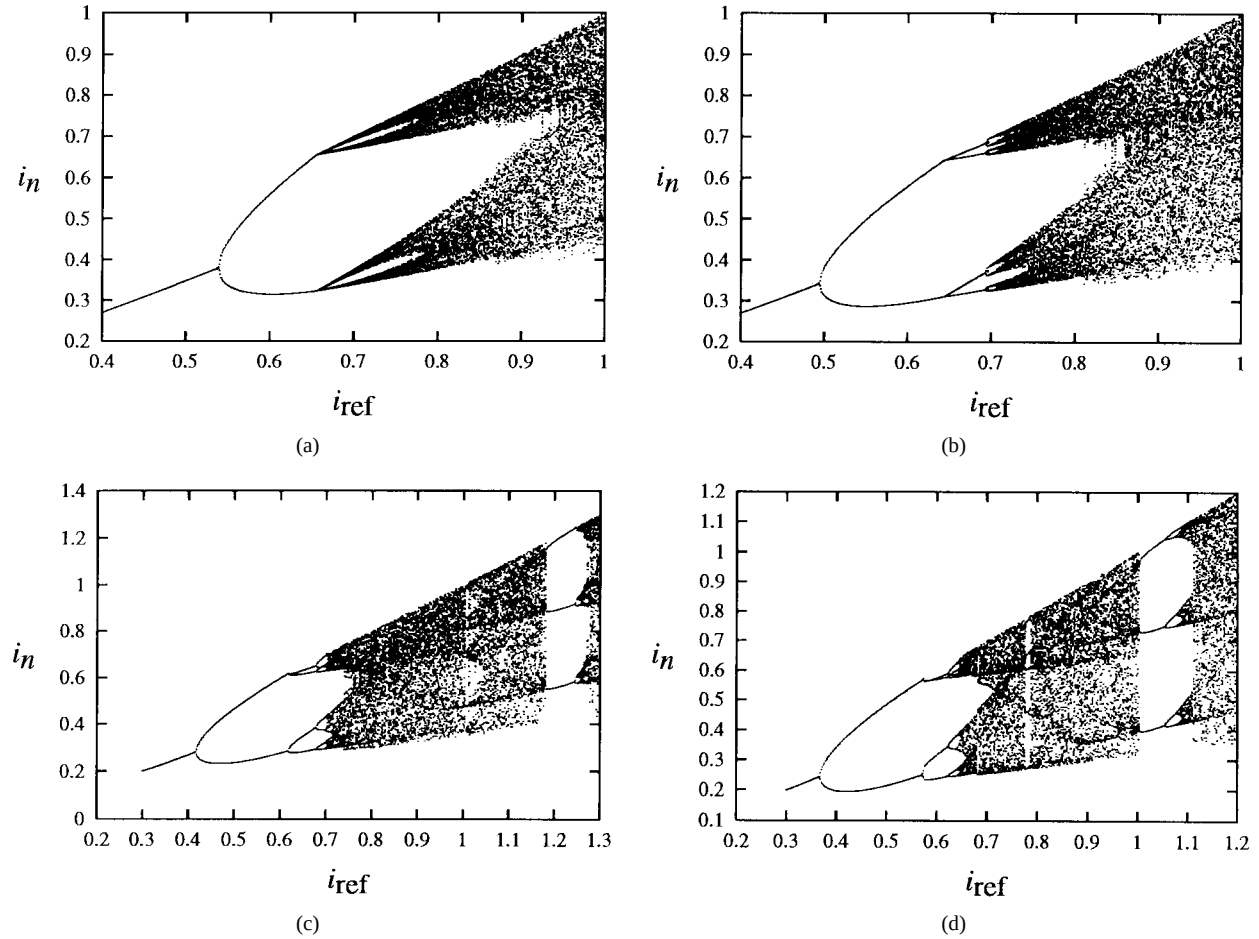

Fig. 13. Bifurcation diagrams from computer simulation of the open-loop circuit. (a) $\gamma = 0.125$, (b) $\gamma = 0.25$, (c) $\gamma = 0.48$, and (d) $\gamma = 0.625$.

VI. The Closed-Loop System

A. Operation of the Closed-Loop Current-Programmed Boost Converter

For power supplies that are used as regulated voltage sources, the mandatory requirement for output voltage regulation necessitates the inclusion of an outer voltage feedback loop. In the case of the current-programmed boost converter, a typical arrangement for incorporating such a feedback loop is shown schematically in Fig. 14. Similar to the open-loop case, the inductance current, as shown in Fig. 15, ramps up until it hits the reference current i_{ref} and ramps down until the switch is turned on by the periodic clock signal. However, in this case, the reference current is controlled by the output voltage according to the following simple feedback scheme:

$$i_{\text{ref}} = I_{\text{ref}} - \kappa[v(nT)e^{-(d_nT/CR)} - V_{\text{ref}}] \qquad (20)$$

where κ is the feedback factor and can be chosen to modify the closed-loop dynamics, V_{ref} is the reference steady-state

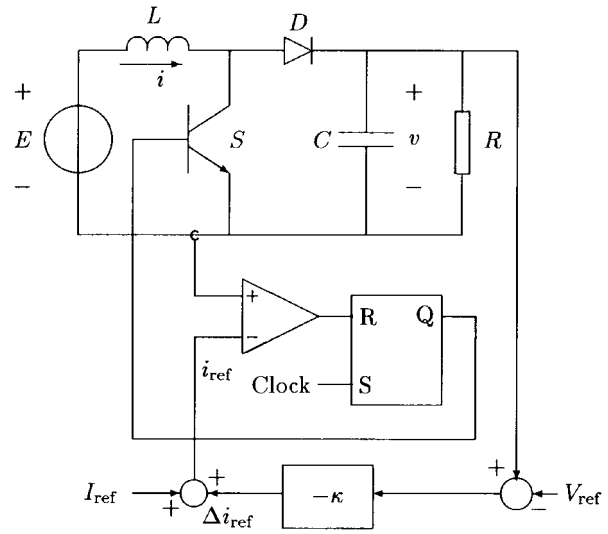

Fig. 14. Schematic diagram of the closed-loop system.

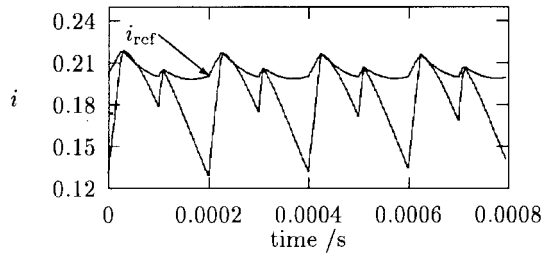

Fig. 15. Waveform of inductance current in the presence of voltage feedback loop.

output voltage, and $I_{\rm ref}$ is the steady-state reference current. Since $d_nT \ll CR$, the following approximation holds:

$$e^{-(d_nT/CR)} \approx 1 - \frac{d_nT}{CR} + \frac{d_n^2T^2}{2C^2R^2}. \tag{21}$$

Also, by inspection of the waveform, we have

$$i_{\rm ref} = \frac{E}{L}\, d_nT + i_n. \tag{22}$$

Finally, solving d_n will allow the difference equation for the closed-loop system to be written as

$$x_{n+1} = f(x_n, \kappa) \tag{23}$$

where x is as previously defined.

B. Bifurcation Parameters

The route to chaos can be predicted from (23) using the analysis method described in Section V. However, in the case of the circuit with an outer voltage feedback loop, $i_{\rm ref}$ is no longer a fixed value that can be selected at will and, hence, is not qualified to serve as a primary bifurcation parameter. Thus, a different set of primary and secondary bifurcation parameters must be used. In our investigation, κ is chosen as the primary bifurcation parameter, and $I_{\rm ref}$ is the secondary bifurcation parameter. With this choice of parameters, we first will study the routes to chaos with respect to variation of κ, and then the bifurcation of the route to chaos with respect to variation of $I_{\rm ref}$.

TABLE III
VALUES OF $I_{\rm ref}$ AND THE CORRESPONDING REFERENCE VOLTAGES

$I_{\rm ref}$	reference voltage $V_{\rm ref}$	corresponding bifurcation diagram
0.2006A	5.96V	Fig. 16 (a)
0.2500A	6.58V	Fig. 16 (b)
0.2918A	7.10V	Fig. 16 (c)
0.3528A	7.83V	Fig. 16 (d)

In developing a bifurcation diagram with respect to variation of κ, we need to keep $I_{\rm ref}$ fixed. In addition, the process requires that the corresponding steady-state value of the output voltage be known and be assigned to $V_{\rm ref}$. Thus, in preparation for the derivation of the bifurcation diagrams, we need to precalculate the values of $V_{\rm ref}$ corresponding to some arbitrarily chosen $I_{\rm ref}$. This can be conveniently accomplished by performing a few simulation runs. Results are given in Table III.

C. Bifurcation Diagrams from Computer Simulations

Similar to the analysis of the open-loop system, two approaches can be taken to derive a series of bifurcation diagrams, as outlined in Sections V-C and V-D. The first approach essentially makes use of an approximate iterative map, which is derived from writing the involving transition matrices as truncated Taylor series, to develop the bifurcation diagrams. The second approach, which is simpler and more straightforward, simulates the required waveforms directly using the exact piecewise switched model and obtains the bifurcation diagrams from the simulated waveforms. In order to keep our presentation in this paper concise, we will omit the iterative map approach for the closed-loop system. Nevertheless, we should stress that both approaches, as demonstrated in Sections V-C and V-D for the open-loop system, will yield essentially the same piece of information regarding the bifurcation of the route to chaos.

The bifurcation diagrams obtained from computer simulations corresponding to the four values of $I_{\rm ref}$ listed in Table III are shown in Fig. 16, from which we clearly see that the route to chaos undergoes exactly the same kind of transition as we last saw in the open-loop system. In other words, the bifurcation phenomena exhibited by the closed-loop system are found to fit the general description outlined by Fig. 9. Moreover, we may conjecture from the above results that Fig. 9 represents a typical bifurcation scenario for the current-programmed dc/dc converter operating in whatever configuration (e.g., open-loop or closed-loop) and with whatever choice of bifurcation parameters that are suitable for the type of configuration concerned.

C. Lyapunov Exponents

In the study of chaotic systems, Lyapunov exponents are often used to identify and quantify chaos. In simple terms, the signs of the Lyapunov exponents determine whether stretching or contracting occurs in a certain direction in the phase space. For a kth order system, there are k Lyapunov exponents, each of which describes the extent of stretching or

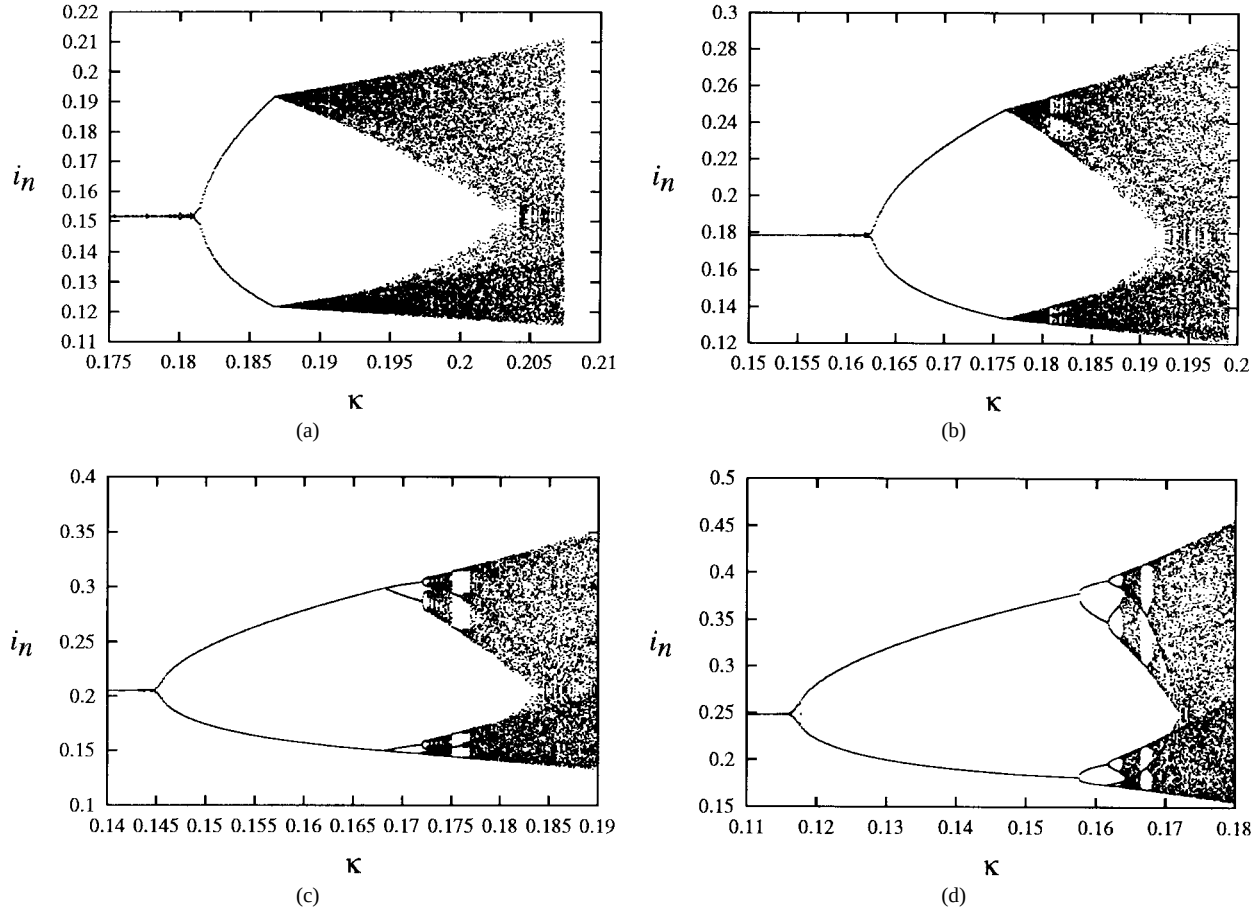

Fig. 16. Bifurcation diagrams from computer simulation of the closed-loop circuit. (a) $I_{\rm ref} = 0.2006$A, (b) $I_{\rm ref} = 0.25$A, (c) $I_{\rm ref} = 0.2918$A, (d) $I_{\rm ref} = 0.3528$A.

contracting in one direction [17]. For stable periodic and subharmonic motions, Lyapunov exponents for all directions must be negative. For quasi-periodic motions, the largest Lyapunov exponent is zero, and for chaotic motions, the largest Lyapunov exponent is positive. Hence, Lyapunov exponents can be used to distinguish between quasi-periodic and chaotic behavior [17].

Mathematically, the Lyapunov exponents ($\lambda_{1\cdot k}$) for a kth order dynamical system are defined by

$$\lambda_i = \lim_{n\to\infty} \frac{1}{n} \log \left| \text{eig} \left\{ \prod_{j=0}^{n} J(x_j) \right\} \right| \tag{24}$$

where $J(x_j)$ is the Jacobian of the system evaluated along the trajectory [17]. If the differential or difference equations defining the system are known, we can apply the above formula to find the Lyapunov exponents. A practical and efficient algorithm, based on the Gram–Schmidt orthonormalization technique, is often employed to calculate λ_i [18]. On the other hand, if the equations that describe the system are not known, we can evaluate the Lyapunov exponents directly from the system's time-domain waveform or sampled time series [19].

For computational simplicity, we have calculated the largest Lyapunov exponent for fundamental and subharmonic regions using the Gram–Schmidt algorithm [18]. For quasi-periodic and chaotic regions, we have resorted to the time series method [19]. Our purpose of calculating the largest Lyapunov exponent here is mainly to verify quasi-periodicity that has been predicted from the bifurcation diagrams and time-domain waveforms. For brevity and to avoid presenting redundant results, we report here our calculations of the largest Lyapunov exponent corresponding to the bifurcation diagram of Fig. 11(a). As shown in Fig. 17, for this particular case, the system exhibits quasi-periodicity in the region around $0.6 < i_{\rm ref} < 0.68$.

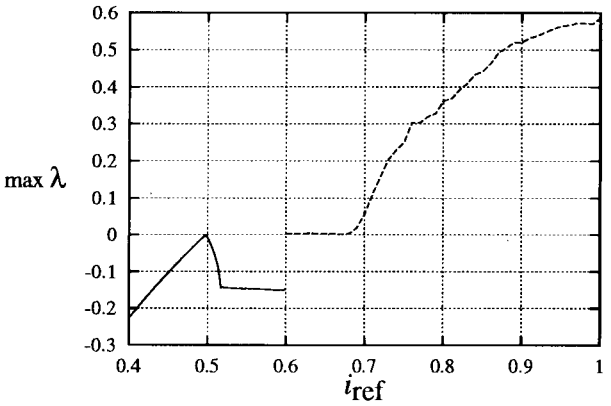

Fig. 17. The largest Lyapunov exponent versus $i_{\rm ref}$, corresponding to Fig. 11(a).

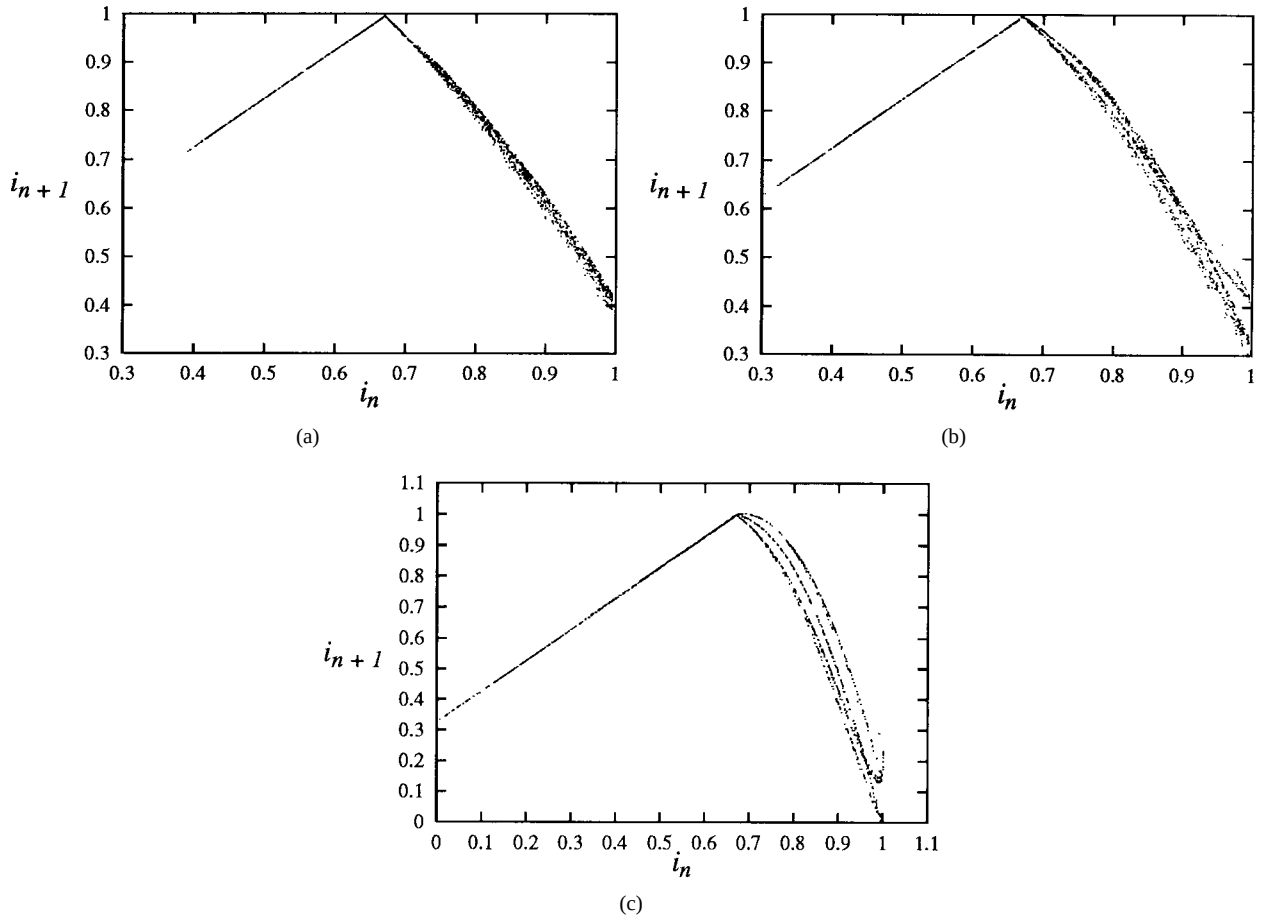

Fig. 18. Return map for (a) Fig. 11(a), (b) Fig. 10(b), and (c) Fig. 11(c).

VII. An Alternative Viewpoint Using Return Maps

Return maps represent very useful tools for analyzing chaotic systems [20], in particular high-order chaotic systems and experimental chaos for which analytical or closed-form iterative functions are difficult to obtain. Essentially, the method allows the dynamics of the system to be summarized by a 1-dim map. Here, we make use of this method to examine the transition of the route to chaos, subject to variation of the secondary bifurcation.

In the previously derived bifurcation diagrams, we have observed that the route to chaos undergoes a region of quasi-periodicity for small values of the secondary bifurcation parameter, and becomes period-doubling for large values of the secondary bifurcation parameter. It would be interesting to see how the appearance of the return map varies as the secondary bifurcation parameter changes, and it would be quite enlightening if we could relate the return maps of the second-order system under study to some familiar 1-dim maps. For instance, period-doubling is often associated with a logistic type of 1-dim maps, and the bifurcation via period-doubling is suppressed in a tent type of 1-dim maps. In the following, we will show that the return maps corresponding to the current-programmed converter in question appear at first as a tent-like map, and as the secondary bifurcation parameter increases, the return maps approach a logistic-like map with an obvious unimodal appearance.

In the process of constructing return maps, we employ (7) and (9) to generate discrete-time values of x at $t = nT$, with the first 1000 transient points discarded. We then plot the points (i_k, i_{k+1}), for $k = 1001$ to 16 000, i.e., 15 000 points plotted. To maintain a concise presentation, we report in Fig. 18 the results for the case of $i_{\text{ref}} = 1$. Here, we clearly observe the qualitative change from a tent-like map to a smooth logistic-like map [21].

VIII. Conclusion

Although very few formal reports have been written about chaos in dc/dc converters, the power-supply engineers have lived with chaos ever since the introduction of dc/dc converters and their overwhelming use in power-supply design. Despite its importance and frequent occurrence, chaos in dc/dc converters is still rarely studied, presumably because the kind of approach required for the study of chaotic dynamics is rather unfamiliar to the power electronics engineers. Up to now, only a few papers have been published on the subject of chaos in dc/dc converters. A recent survey of published work in this area can be found in [22].

This paper focuses in particular on the current-programmed boost converter and attempts to put together the few isolated results reported previously on the routes to chaos exhibited by such systems. Specifically, previous studies have identified two types of route to chaos, namely via regions of quasi-

periodicity and via period-doubling [6]–[10]. In this paper, we have shown that the bifurcation path exhibited by a current-programmed dc/dc converter with respect to variation of a primary bifurcation parameter undergoes a bifurcation with respect to variation of a secondary bifurcation parameter, starting from one that goes through quasi-$4T$-periodic orbits via progressively longer quasi-periodic orbits, eventually to period-doubling. We conclude this paper by reiterating our conjecture that such a bifurcation is characteristic of current-programmed dc/dc converters, and as long as a suitable set of bifurcation parameters is chosen, the route to chaos will exhibit this typical bifurcation.

APPENDIX

Expressions for the matrix elements in the iterative map derived in Section IV are summarized below. For brevity, we define $t_c = d_n T$ and $t_d = (1-d_n)T$. All other symbols are consistent with those given in the paper:

$$f_{11} = \left(1 - \frac{t_c}{CR} + \frac{t_c^2}{2C^2R^2}\right)\left[1 - \frac{t_d}{CR} + \frac{t_d^2}{2}\left(\frac{1}{C^2R^2} - \frac{1}{LC}\right)\right]$$

$$f_{12} = \frac{t_d}{C} - \frac{t_d^2}{2C^2R}$$

$$f_{21} = \left(1 - \frac{t_c}{CR} + \frac{t_c^2}{2C^2R^2}\right)\left(-\frac{t_d}{L} + \frac{t_d^2}{2LCR}\right)$$

$$f_{22} = 1 - \frac{t_d^2}{2LC}$$

$$g_1 = \left(\frac{t_d}{C} - \frac{t_d^2}{2C^2R}\right)\left(\frac{t_c}{L}\right) - \left[1 - \frac{t_d}{CR} + \frac{t_d^2}{2}\left(\frac{1}{C^2R^2} - \frac{1}{LC}\right)\right] \cdot \left[\frac{t_d^2(3CR + t_d)}{6C^2LR}\right] + \left(\frac{t_d}{C} - \frac{t_d^2}{2C^2R}\right) \cdot \left[\frac{-t_d(-6CL + T^2 - 2Tt_c + tc^2)}{6CL^2}\right]$$

$$g_2 = \left(1 - \frac{t_d^2}{2LC}\right)\left(\frac{t_c}{L}\right) - \left(-\frac{t_d}{L} + \frac{t_d^2}{2CLR}\right) \cdot \left[\frac{t_d^2(3CR + t_d)}{6C^2LR}\right] + \left(1 - \frac{t_d^2}{2LC}\right) \cdot \left[\frac{-t_d(-6CL + T^2 - 2Tt_c + tc^2)}{6CL^2}\right].$$

ACKNOWLEDGMENT

The authors wish to thank the anonymous reviewers for their comments and suggestions which helped to improve the content of this paper.

REFERENCES

[1] A. Capel, G. Ferrante, D. O'Sullivan, and A. Weinberg, "Application of the injected current model for the dynamic analysis of switching regulators with the new concept of LC^3 modulator," in *IEEE Power Electron. Specialists Conf. Rec.*, Syracuse, NY, June 1978, pp. 135–147.

[2] F. C. Lee and R. A. Carter, "Investigations of stability and dynamic performances of switching regulators employing current-injected control," in *IEEE Power Electron. Specialists Conf. Rec.*, June 1981, pp. 3–16.

[3] R. D. Middlebrook, "Topics in multiple-loop regulators and current-mode programming," in *IEEE Power Electron. Specialists Conf. Rec.*, Toulouse, France, June 1985, pp. 716–732.

[4] D. M. Mitchell, "An analytical investigation of current-injected control for constant frequency switching regulators," in *IEEE Power Electron. Specialists Conf. Rec.*, 1985, pp. 225–233.

[5] R. Redl and N. Sokal, "Current-mode control, five different types, used with the three basic classes of power converters," in *IEEE Power Electron. Specialists Conf. Rec.*, 1985, pp. 771–785.

[6] C. K. Tse and W. C. Y. Chan, "Chaos from a current programmed Ćuk converter," *Int. J. Circuit Theory Appl.*, vol. 23, pp. 217–225, May–June 1995.

[7] ——, "Instability and chaos in a current-mode controlled Ćuk converter," in *IEEE Power Electron. Specialists Conf. Rec.*, Atlanta, GA, June 1995, pp. 608–613.

[8] I. Zafrany and S. Ben-Yaakov, "A chaos model of subharmonic oscillations in current mode PWM boost converters," in *IEEE Power Electron. Specialists Conf. Rec.*, Atlanta, GA, June 1995, pp. 1111–1117.

[9] J. H. B. Deane and D. C. Hamill, "Chaotic behavior in current-mode controlled dc/dc converters," *Inst. Elect. Eng. Electron. Lett.*, vol. 27, no. 13, pp. 1172–1173, June 1991.

[10] J. H. B. Deane, "Chaos in a current-mode controlled boost dc/dc converter," *IEEE Trans. Circuits Syst. I*, vol. 39, pp. 680–683, Aug. 1992.

[11] W. C. Y. Chan and C. K. Tse, "A universal bifurcation path conjectured from current-programmed switching converters," in *Proc. Int. Symp. Nonlinear Theory Appl.*, Rochi, Japan, Oct. 1996, pp. 121–124.

[12] ——, "Studies of routes to chaos current-programmed dc/dc converters," in *IEEE Power Electron. Specialists Conf. Rec.*, Baveno, Italy, June 1996, pp. 789–795.

[13] ——, "Bifurcations in current-programmed dc/dc buck switching regulators—Conjecturing a universal bifurcation path," *Int. J. Circuit Theory Appl.*, to be published.

[14] T. S. Parker and L. O. Chua, *Practical Numerical Algorithims for Chaotic Systems.* Berlin, Germany: Springer-Verlag, 1989.

[15] S. Jalali, I. Dobson, R. H. Lasseter, and G. Venkataramanan, "Switching time bifurcations in a thyristor controlled reactor," *IEEE Trans. Circuits Syst. I*, vol. 43, pp. 209–218, Mar. 1996.

[16] Y. A. Kuznetsov, *Elements of Applied Bifurcation Theory.* Berlin, Germany: Springer-Verlag, 1996.

[17] R. C. Hilborn, *Chaos and Nonlinear Dynamics.* London, U.K.: Oxford University Press, 1994.

[18] H. Peitgen, H. Jürgens, and D. Saupe, *Chaos and Fractals—New Frontiers of Science.* Berlin, Germany: Springer-Verlag, 1992.

[19] A. Wolf, J. B. Swift, H. L. Swinney, and J. A. Vastano, "Determining Lyapunov exponents from a time series," *Physics D*, vol. 16, pp. 285–317, 1985.

[20] R. H. Simoyi, A. Wolf, and H. L. Swinney, "One dimensional dynamics in a multicomponent chemical reaction," *Phys. Rev. Lett.*, vol. 49, pp. 245–248, 1982.

[21] S. N. Rashand, *Chaotic Dynamics of Nonlinear Systems.* New York: Wiley, 1990.

[22] D. C. Hamill, "Power electronics: A field rich in nonlinear dynamics," presented at the *Int. Workshop Nonlinear Dynamics Electron. Syst.*, Dublin, Ireland, July 1995.

William C. Y. Chan received the B.S. degree in engineering physics with first class honors from Hong Kong Polytechnic University, Hung Hom, Hong Kong, in 1994, and is currently working toward the Ph.D. degree in electronic engineering.

His main research interests include the identification and theoretical study of chaotic behavior of power electronics. He has co-authored 10 technical papers in this area.

Mr. Chan was the recipient of the Sir Edward Youde Memorial Fellowship awarded by the Sir Edward Youde Memorial Council, Hong Kong, in 1997.

Chi K. Tse (M'90–SM'97), for a photograph and biography, see p. 675 of the August 1997 issue of this TRANSACTIONS.